Distance-dependent regulation of NMDAR nanoscale organization along hippocampal neuron dendrites

Joana S. Ferreira[a,b,1], Julien P. Dupuis[a,b], Blanka Kellermayer[a,b], Nathan Bénac[a,b], Constance Manso[a,b], Delphine Bouchet[a,b], Florian Levet[a,b,c,d,e], Corey Butler[a,b], Jean-Baptiste Sibarita[a,b], and Laurent Groc[a,b,1]

[a]Interdisciplinary Institute for Neuroscience, University of Bordeaux, UMR 5297, 33076 Bordeaux, France; [b]CNRS, IINS UMR 5297, Bordeaux, France; [c]Bordeaux Imaging Center, University of Bordeaux, 33076 Bordeaux, France; [d]Bordeaux Imaging Center, CNRS UMS 3420, 33076 Bordeaux, France; and [e]Bordeaux Imaging Center, INSERM US04, 33076 Bordeaux, France

Edited by Richard L. Huganir, Johns Hopkins University School of Medicine, Baltimore, MD, and approved August 10, 2020 (received for review December 20, 2019)

Hippocampal pyramidal neurons are characterized by a unique arborization subdivided in segregated dendritic domains receiving distinct excitatory synaptic inputs with specific properties and plasticity rules that shape their respective contributions to synaptic integration and action potential firing. Although the basal regulation and plastic range of proximal and distal synapses are known to be different, the composition and nanoscale organization of key synaptic proteins at these inputs remains largely elusive. Here we used superresolution imaging and single nanoparticle tracking in rat hippocampal neurons to unveil the nanoscale topography of native GluN2A- and GluN2B-NMDA receptors (NMDARs)—which play key roles in the use-dependent adaptation of glutamatergic synapses—along the dendritic arbor. We report significant changes in the nanoscale organization of GluN2B-NMDARs between proximal and distal dendritic segments, whereas the topography of GluN2A-NMDARs remains similar along the dendritic tree. Remarkably, the nanoscale organization of GluN2B-NMDARs at proximal segments depends on their interaction with calcium/calmodulin-dependent protein kinase II (CaMKII), which is not the case at distal segments. Collectively, our data reveal that the nanoscale organization of NMDARs changes along dendritic segments in a subtype-specific manner and is shaped by the interplay with CaMKII at proximal dendritic segments, shedding light on our understanding of the functional diversity of hippocampal glutamatergic synapses.

super-resolution | GluN2B-NMDA receptor | dendrite | dSTORM

Encoding and storage of memories in the hippocampus requires the simultaneous collection of information from several coactive brain areas during sensory experience. At the cellular level, this procedure occurs through the integration by pyramidal neurons, the principal cells of the hippocampus, of synaptic inputs coinciding in time and/or space to shape neuronal firing. Illustrating this complexity, hippocampal CA1 pyramidal neurons receive sensory information through distal excitatory inputs from the entorhinal cortex and proximal indirect excitatory inputs from the hippocampal CA3 area distributed along an elaborated dendritic arbor with synapses sometimes located hundreds of microns away from the soma (1–4). How this multiplicity of inputs combines to shape the firing activity of pyramidal neurons, and how sensory experience dynamically changes their respective weight to allow memory encoding and storage are challenging questions. While distance-dependent filtering of signal propagation would be expected to blunt the contribution of distal synapses to neuronal activity (5, 6), local synaptic and dendritic compensatory mechanisms, such as scaling in the number of alpha-amino-3-hydroxy-5-methyl-4-isoxazole propionic acid glutamate receptors (AMPARs) mediating fast glutamatergic neurotransmission allow to offset the location dependence of synaptic influence, suggesting that a fine control of local glutamate receptor expression and organization actively ensures the integration properties of pyramidal neurons (7–16).

Furthermore, the relative influence of glutamatergic inputs on the firing activity of pyramidal neurons is dynamically tuned by plasticity processes that happen to be remarkably different at proximal and distal synapses. Calcium-permeant *N*-methyl-D-aspartate glutamate receptors (NMDARs) are central actors in these adaptations, strengthening or weakening excitatory inputs. NMDARs are heterotetrameric cationic channels resulting from the combination of two obligatory GluN1 subunits with two GluN2 (A, D) and/or GluN3 (A, B) subunits (17). CA1 pyramidal neurons predominantly express GluN2A and GluN2B subunit-containing receptors, which display specific biophysical, pharmacologic, trafficking, and signaling properties. Importantly, the relative abundance of GluN2A- and GluN2B-NMDARs shapes the range of activity-dependent long-term synaptic adaptations supporting neuronal network maturation and adaptation (18–28). In particular, the recruitment and activation of the Ca^{2+}/calmodulin-dependent protein kinase II (CaMKII) to dendritic spines by GluN2B-NMDARs appear to be critical steps in the induction of long-term potentiation (LTP) and the formation of new memories (29–36).

Unlike AMPAR, expression levels of NMDARs remain relatively stable along the dendritic arborization of CA1 pyramidal neurons (11, 37). However, the relative abundances of GluN2A- and GluN2B-NMDARs diverge significantly depending on the type of input, and NMDAR-mediated synaptic calcium influxes increase with distance from the soma (15, 37–41). Indeed, GluN2A-NMDARs predominate at distal inputs from the

Significance

Glutamatergic synapses onto pyramidal neurons are diverse in shape, size, and NMDAR-dependent long-term plasticity according to their dendritic location, i.e., proximal or distal to the soma. Deciphering the fine organization of NMDAR subtypes along the dendritic arbor of hippocampal neurons is key to understand the functional diversity of these various synapses. We unveil that the nanoscale organization of NMDAR changes as a function of distance from the soma in a subunit-specific and CaMKII interaction-dependent manner at proximal dendritic segments.

Author contributions: J.S.F. and L.G. designed research; J.S.F., J.P.D., B.K., N.B., C.M., and D.B. performed research; C.M., D.B., F.L., C.B., and J.-B.S. contributed new reagents/analytic tools; J.S.F., J.P.D., B.K., and N.B. analyzed data; and J.S.F., J.P.D. and L.G. wrote the paper.

The authors declare no competing interest.

This article is a PNAS Direct Submission.

[1]To whom correspondence may be addressed. Email: joana.ferreira@u-bordeaux.fr or laurent.groc@u-bordeaux.fr.

This article contains supporting information online at https://www.pnas.org/lookup/suppl/doi:10.1073/pnas.1922477117/-/DCSupplemental.

First published September 14, 2020.

entorhinal cortex when GluN2B-NMDARs are in the majority at proximal inputs from the CA3 area. Thus affects the activity-dependent changes in the strength of these synapses and on their respective contributions to neuronal activity, with proximal inputs more prone to express NMDAR-dependent LTP than distal inputs whereas the opposite holds for NMDAR-dependent long-term depression (LTD) (38–40, 42–47). Interestingly, these input-specific features appear to be cell-autonomous and persist in dissociated neurons (15, 37); however, how they emerge remains an open question.

The recent development of superresolution microscopy revealed that the nanoscale organization of molecular actors at presynaptic and postsynaptic compartments plays a major role in controlling the efficacy and plasticity of glutamatergic synaptic transmissions (48–57). Here we combined superresolution imaging, single-particle tracking, and glutamate uncaging approaches to investigate whether local variations in the nanoscale organizations of GluN2A- and GluN2B-containing NMDARs and their signaling partners may contribute to the diversity of synaptic properties observed along the apical dendritic tree of hippocampal neurons. We reveal that the nanoscale organization of synaptic GluN2B-NMDARs changes with distance from the soma in a process regulated by the functional and physical interplay with CaMKII.

Results

Distance-Dependent Regulation of GluN2-NMDAR Nanoscale Organization and Stabilization. To explore the nanoscale organization of the two predominant NMDAR subtypes expressed along the apical dendrites of hippocampal pyramidal neurons, we first performed live immunostaining with antibodies selective for either GluN2A- or GluN2B-NMDAR subunits (54) (Fig. 1*A*). As described previously (11, 37, 58, 59), we observed a distance-dependent decrease in the size of dendritic spines, using GFP-Homer expression as a synaptic marker (*SI Appendix*, Fig. S1*A*). Using soluble GFP expression as a neuronal filling marker, proximal dendrites (defined as <40 μm away from the soma) and distal dendrites (defined as >80 μm away from the soma) were sequentially imaged by dSTORM (Fig. 1*A*). Receptor clusters and nanodomains were segmented and quantified using tessellation-based segmentation (60), as reported previously (54) (Fig. 1*B*). The linear densities of epifluorescent clusters of GluN2A- and GluN2B-NMDARs were not significantly different (mean ± SEM, GluN2A: 1.6 ± 0.35 clusters/μm, $n = 8$ cells; GluN2B: 1.8 ± 0.3 clusters/μm, $n =$ 10 cells), nor were the linear densities of clusters of either subtype when comparing proximal and distal dendritic segments (*SI Appendix*, Fig. S1*B*). The nanoscale organization of GluN2A-NMDARs was relatively stable throughout the dendritic tree, with similar cluster and nanodomain areas as well as the number of localizations per cluster at proximal and distal dendritic segments (Fig. 1 *C–F* and *SI Appendix*, Fig. S1*C*), although local densities (#localizations/area) of GluN2A-NMDAR clusters and nanodomains increased with distance (*SI Appendix*, Fig. S1*D*). Of note, GluN2A-NMDARs showed a decrease in the number of nanodomains per cluster at distal segments (*SI Appendix*, Fig. S1*E*) which was associated with a 2.3-fold increase in the number of localizations per nanodomain (Fig. 1*E* and *SI Appendix*, Table S1). In contrast, we observed larger distance-dependent variations in GluN2B-NMDAR nanoscale organization with a significant drop in the area of clusters and nanodomains at distal locations that was associated with an increase in the number of localizations for both parameters, resulting in a 1.9-fold and 2.4-fold net increase in the local densities (#localizations/area) of distal GluN2B-NMDAR clusters and nanodomains, respectively (Fig. 1 *C–F* and *SI Appendix*, Table S1). GluN2B-NMDAR clusters were also more heterogeneous than GluN2A-NMDAR clusters at both proximal and distal segments, as suggested by a greater dispersion in the frequency distributions of their localizations per cluster (*SI Appendix*, Fig. S1*C*).

Using single nanoparticle tracking, we next assessed whether these distance-dependent nanoscale organization properties were paralleled by differences in receptor surface dynamics at proximal and distal synapses (Fig. 1*F*). While the diffusion properties of synaptic YFP-GluN2A-NMDARs were comparable at proximal and distal segments, we observed a significant decrease in instantaneous surface diffusion coefficients together with a twofold increase in the synaptic residency time of YFP-GluN2B-NMDARs at distal synapses compared with proximal synapses (Fig. 1*G* and *SI Appendix*, Table S1), indicating that GluN2B-NMDARs are less efficiently trapped at proximal synapses.

Taken together, our results show that the nanoscopic distribution and synaptic dynamics of NMDARs evolve in a subunit-dependent manner as a function of distance along the dendrites of hippocampal neurons. While the organization and synaptic stabilization of GluN2A-NMDARs are relatively stable throughout the dendritic tree, local densities of GluN2B-NMDAR clusters and nanodomains, as well as synaptic stabilization are enhanced at distal synapses, possibly through local changes in signaling or interactions with scaffolding partners (54, 61).

Binding to CaMKII Sculpts the Nanoscale Organization and Dynamics of GluN2B-NMDARs. We then explored the possible mechanisms that contribute to the distance-dependent changes in the nanoscale organization of GluN2B-NMDARs. One of the powerful regulators of GluN2B-NMDARs is CaMKII, which is known to bind this receptor subtype with high affinity upon activation and to affect its signaling and surface trafficking properties (29, 35, 62). We investigated whether CaMKII also differentially organizes along the dendritic tree. To this end, hippocampal neurons were transfected with GFP-labeled CaMKII, whose nanoscale organization was defined using dSTORM (Fig. 2 *A* and *C* and *SI Appendix*, Fig. S2*A*). As suggested previously (63), CaMKII density was lower at distal spines compared with proximal ones (Fig. 2*B* and *SI Appendix*, Table S1). CaMKII did not appear to form nanodomains under basal conditions; out of 193 identified clusters, 131 were totally devoid of nanodomains. Moreover, 89% of the clusters in which a nanostructuration was identified displayed one nanodomain only, which filled the center of the cluster (Fig. 2*C*). Therefore, we focused our analysis on cluster characteristics (Fig. 2*D* and *SI Appendix*, Fig. S2*B*). The number of localizations per cluster was substantially lower at distal segments (*SI Appendix*, Fig. S2*B* and Table S1) and was associated with a threefold reduction in the local density of CaMKII clusters (Fig. 2*D* and *SI Appendix*, Fig. S2*B* and Table S1). Thus, CaMKII cluster density is high at proximal synapses where GluN2B-NMDARs display low density and high surface dynamics.

To investigate whether an interplay exists between CaMKII and GluN2B-NMDAR nanoscale organization, we transfected and imaged hippocampal neurons with either wild-type GluN2B (WT) or a recombinant GluN2B that is impaired for CaMKII binding (GluN2B-RSQD) (31) and imaged the distribution of these receptors using dSTORM (Fig. 2*E*). As described previously (31), WT and mutant receptors were expressed at similar levels and did not affect the distance-dependent decrease in spine size toward distal locations (*SI Appendix*, Fig. S2*C*). Moreover, the distributions of the localizations per cluster revealed a similar cluster heterogeneity in recombinant GluN2B-WT as in endogenous GluN2B-NMDAR (*SI Appendix*, Fig. S2*D*). Remarkably, the inability to bind CaMKII impacted the distribution of GluN2B-NMDARs at proximal dendritic segments (Fig. 2*F* and *SI Appendix*, Fig. S2 *F* and *G*). Indeed, the local density of GluN2B-RSQD clusters was increased (Fig. 2*F* and *SI Appendix*, Table S1) as a result of an enhanced number of localizations per cluster (*SI Appendix*, Fig. S2*F* and Table S1). Concomitantly, the local density of GluN2B-RSQD nanodomains was also increased at proximal segments compared with WT GluN2B (Fig. 2*F* and *SI Appendix*, Table S1). The local density of GluN2B-RSQD nanodomains was also increased at distal dendrites, with no significant changes in the nanodomain

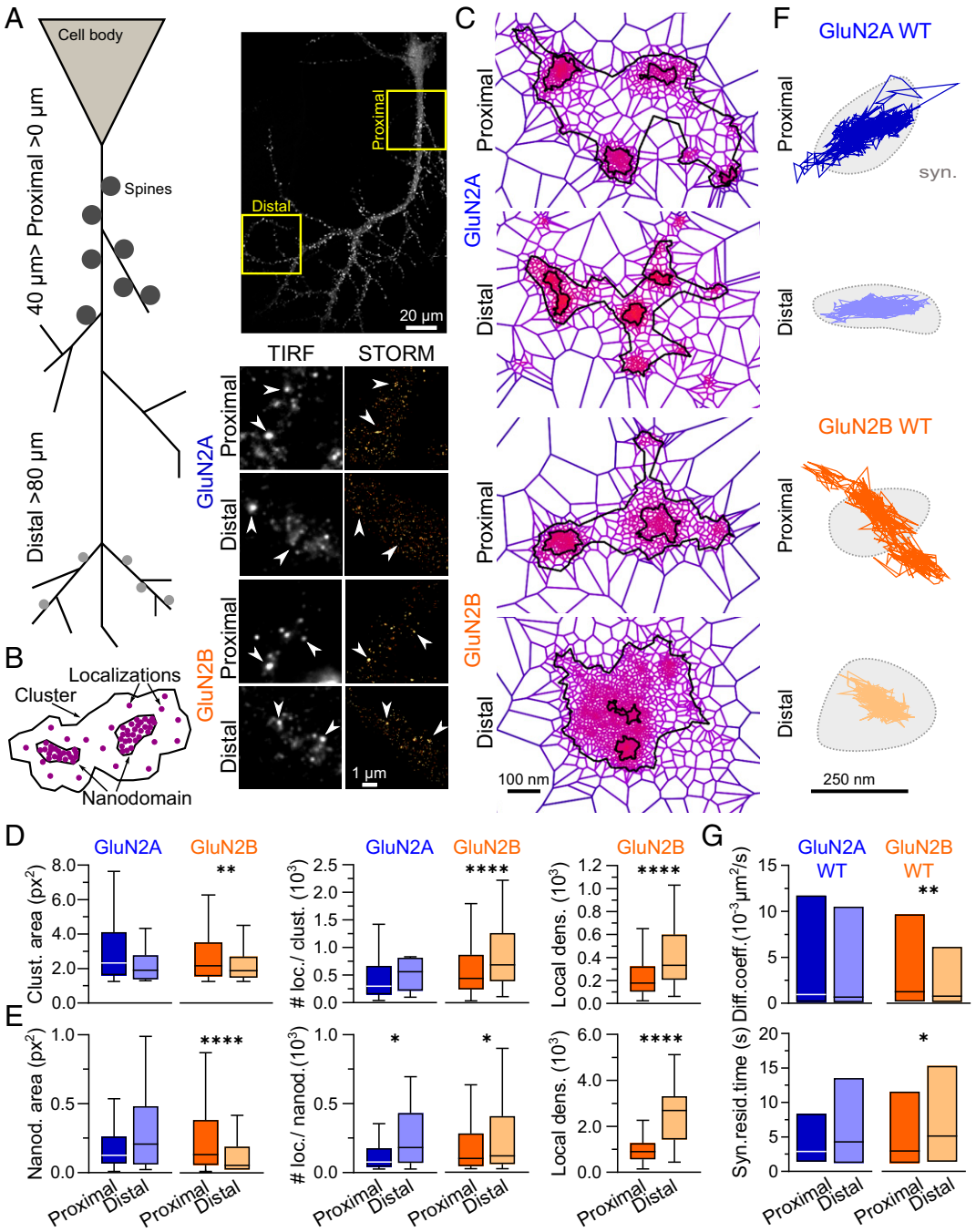

Fig. 1. The nanoscale organization and diffusion properties of GluN2B-NMDARs change in a distance-dependent manner along the dendritic tree of pyramidal neurons. (*A*, *Top Left*) Representation of a schematic hippocampal pyramidal neuron and its dendritic arborization with proximal and distal segments. (*A*, *Top Right*) Hippocampal neurons expressing the GluN2B subunit (*insets*) represent imaging regions defined as proximal (0-40 µm from cell body) and distal (>80 µm from cell body). (*A*, *Bottom Right*) Representative images of GluN2A-NMDARs and GluN2B-NMDARs in low resolution, imaged with total internal reflection fluorescence (TIRF) microscopy (black and white panels), and the corresponding high-resolution image obtained with direct stochastic optical reconstruction microscopy (STORM; gold pseudocolor panels). (*B*) Representative drawing scheme of a NMDAR cluster segmentation resulting from SR-Tesseler analysis. (*C*) Representative clusters of endogenous GluN2A-NMDAR (*Top*) and GluN2B-NMDAR (*Bottom*) at proximal (*Upper*) or distal (*Lower*) dendritic segments obtained with SR-Tesseler. (*D*) Comparison of proximal and distal GluN2A- and GluN2B-NMDAR cluster areas (Clust. area; *Left*) and number of localizations per cluster (# loc./clust.; *Middle*). The local density of GluN2B-NMDAR clusters (Local dens.; *Right*) corresponds to the number of localizations per cluster divided by the respective area (in px^2). (*E*) Comparison between proximal and distal GluN2A- and GluN2B-NMDAR nanodomain areas (Nanod. area; *Left*) and number of localizations per nanodomain (# loc./nanod.; *Middle*). The local density of GluN2B-NMDAR nanodomains (Local dens.; *Left*) corresponds to the number of localizations per nanodomain divided by the respective area (in px^2). Data are represented as box-and-whisker plots: line at median, IQR in box, whiskers represent minimum and maximum values. (*F*) Representative surface trajectories of WT YFP-GluN2A (GluN2A WT; blue) and YFP-GluN2B (GluN2B WT; orange) within proximal (*Top*) and distal (*Bottom*) synapses (identified as Homer-DsRed–positive clusters; light gray), obtained using single nanoparticle (Quantum Dot 655 [QD]) tracking. (*G*) Comparison between proximal (dark colors) and distal (light colors) QD-GluN2A-WT- and QD-GluN2B-WT-NMDAR diffusion coefficients (Diff. coeff.; *Top*) and synaptic residency times (Syn. resid. time; *Bottom*). Data are presented as median ± IQR. $*P \leq 0.05$; $**P \leq 0.01$; $****P \leq 0.0001$; no symbol, $P > 0.05$. Statistical details are provided in *SI Appendix*, Table S1.

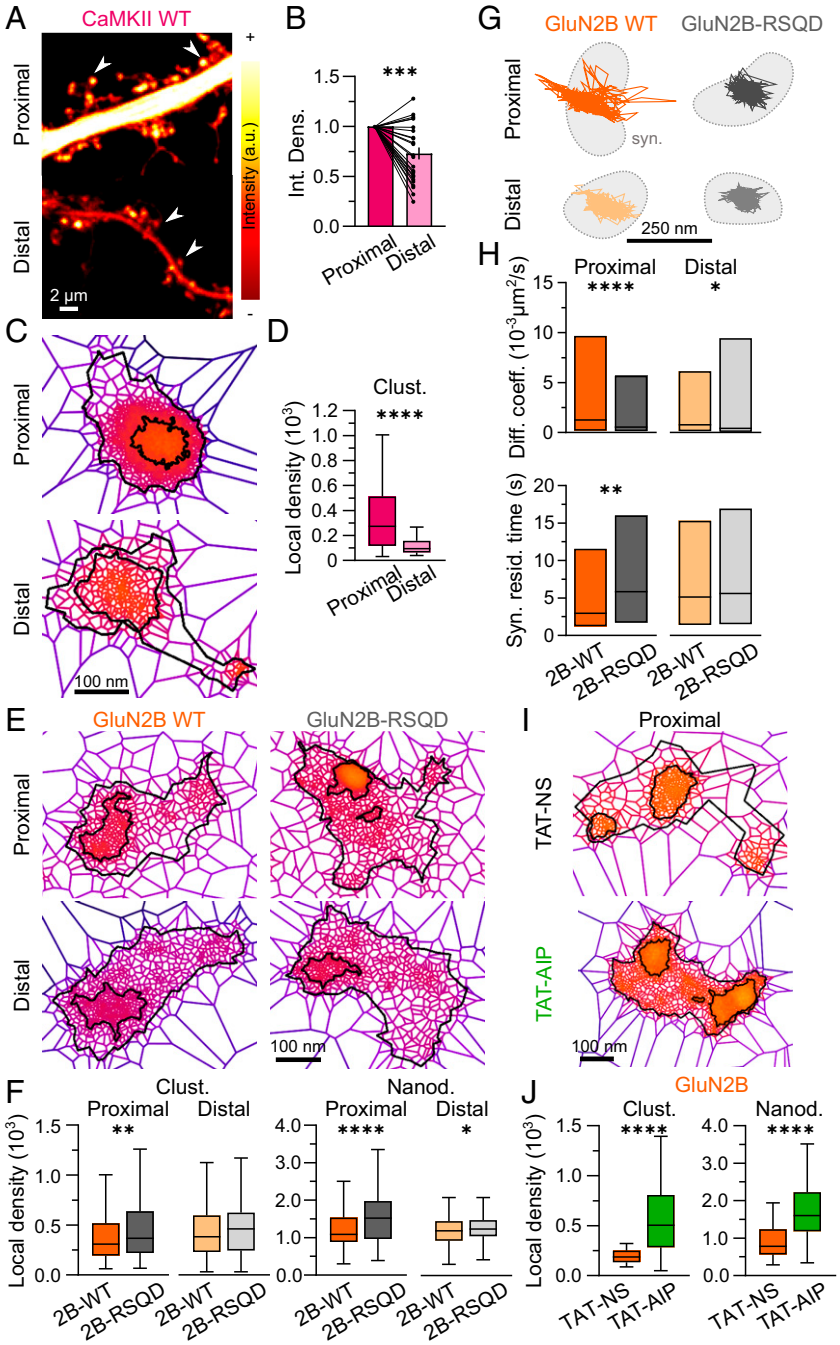

Fig. 2. GluN2B-NMDAR interplay with CaMKII specifically shapes the nanoscale organization and dynamics of receptors at proximal segments. (*A*) Representative confocal images of proximal (*Top*) and distal (*Bottom*) dendritic sections of hippocampal neurons expressing WT GFP-CaMKII *(CaMKII WT*). The pseudocolor gradient reflects differences in intensity (white, higher; red, lower). (*B*) Integrated density (mean intensity normalized to the area of the region of interest) of CaMKII WT in proximal (dark color) or distal (light color) dendritic spines. Data are presented as individual values normalized to proximal segments; line at the mean. (*C*) Representative CaMKII WT clusters within proximal (*Top*) and distal (*Bottom*) dendritic segments obtained by SR-Tesseler analysis. (*D*) Local densities of CaMKII WT clusters at proximal (dark color) and distal (light color) dendritic segments. (*E*) Representative WT YFP-GluN2B (GluN2B WT; *Left)* and CaMKII-binding mutant YFP-GluN2B-RSQD (GluN2B-RSQD; *Right*) clusters within proximal (*Top*) and distal (*Bottom*) dendritic segments obtained by SR-Tesseler analysis. (*F*) Comparison of proximal (dark colors) or distal (light colors) local densities of WT YFP-GluN2B (2B-WT; orange) and mutant YFP-GluN2B-RSQD (2B-RSQD; gray) clusters (*Right*) and nanodomains (*Left*). Data are presented as box-and-whisker plots: line at median, IQR in box, whiskers represent minimum and maximum values. (*G*) Representative surface trajectories of WT YFP-GluN2B (GluN2B WT; orange) and mutant YFP-GluN2B-RSQD (GluN2B-RSQD; gray) within proximal (*Top*; dark colors) and distal (*Bottom*; light colors) synapses (identified as Homer-DsRed–positive clusters; light gray), obtained using single nanoparticle tracking. (*H*) Comparison between proximal (dark colors) and distal (light colors) QD-YFP-GluN2B-NMDAR (*2B-WT*; orange) and QD-YFP-GluN2B-RSQD-NMDAR (*2B-RSQD*; gray) diffusion coefficients (Diff. coeff.; *Top*) and synaptic residency times (Syn. resid. time; *Bottom*). Data are presented as median ± IQR. (*I*) Representative GluN2B-NMDAR clusters after incubation with a control peptide (TAT-NS; *Top)* or a CaMKII inhibitor peptide (TAT-AIP; *Bottom*). (*J*) Local densities of GluN2B-NMDAR clusters and nanodomains at proximal segments after exposure to TAT-NS (orange) or TAT-AIP (green). Data are presented as box-and-whisker plots: line at median, IQR in box, whiskers represent minimum and maximum values. $*P \leq 0.05$; $**P \leq 0.01$; $***P \leq 0.001$; $****P \leq 0.0001$; no symbol, $P > 0.05$. Statistical details are provided in *SI Appendix*, Table S1.

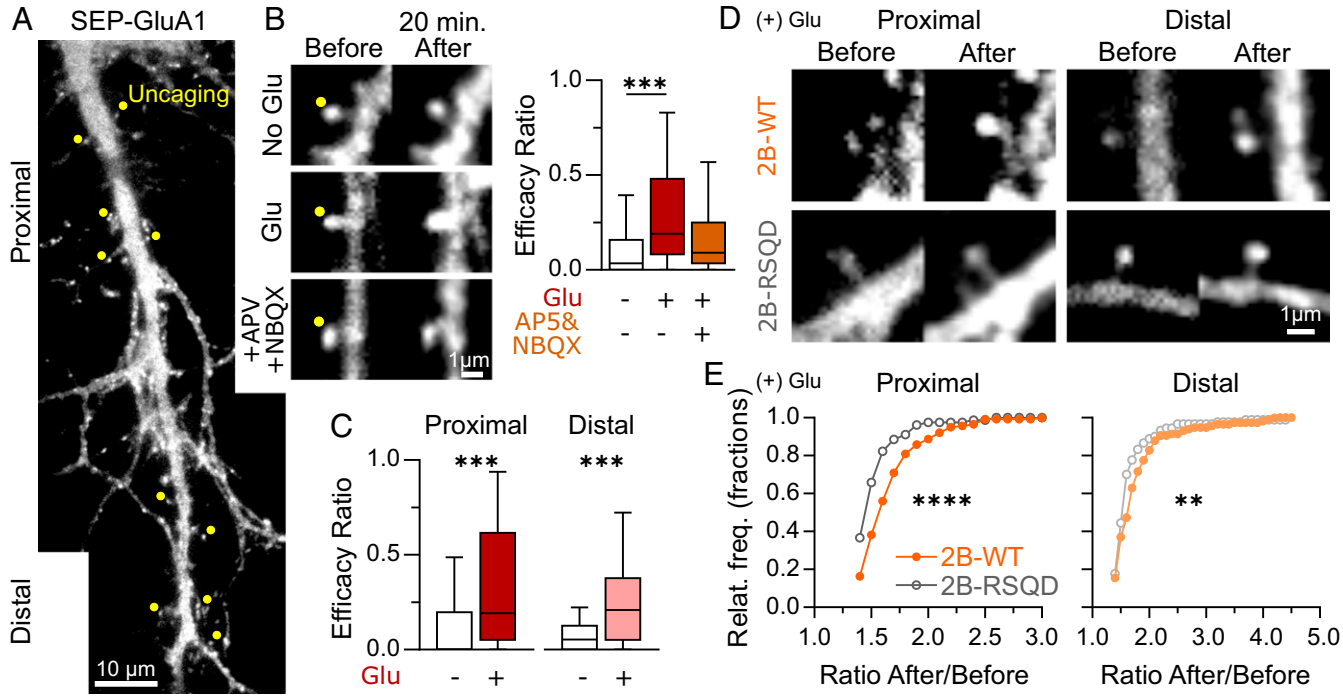

Fig. 3. GluN2B-NMDAR and CaMKII interplay differently impacts LTP depending on distance to the cell soma. (*A*) Representative image of the dendrites of a SEP-GluA1-transfected hippocampal neuron. Yellow dots indicate the spines selected for uncaging. (*B*, *Left*) Representative spines before (*Left*) and 20 min after laser uncaging (*Right*) in the presence of either buffer (without glutamate [no Glu]), caged-glutamate alone (Glu), and caged-glutamate plus glutamate receptor antagonists (*AP5* and *NBQX*). (*B*, *Right*) Efficacy ratio (number of potentiated spines/total number of uncaged spines; *Middle*) in no glutamate (black), glutamate (red), and glutamate plus APV and NBQX (brown) conditions. (*C*) Efficacy ratio at spines located in proximal (dark colors) and distal (light colors) dendritic segments in no glutamate (black) or glutamate (red) conditions. Data are presented as box-and-whisker plots: line at median, IQR in box, whiskers represent minimum and maximum values. (*D*) Representative spines before and after MNI-glutamate uncaging (+ Glu) of SEP-GluA1–transfected neurons coexpressing WT mCherry-GluN2B (2B-WT; *Top*) or the CaMKII binding-deficient mutant mCherry-GluN2B-RSQD (2B-RSQD; *Bottom*) at proximal (*Left*) or distal (*Right*) dendritic segments. (*E*) Relative frequency distributions (Relat. freq.) of after/before SEP-GluA1 fluorescence mean intensity ratio of WT mCherry-GluN2B-NMDAR (2B-WT; orange) and mCherry-GluN2B-RSQD-NMDAR (2B-RSQD; gray) transfected hippocampal neurons at proximal (dark colors; *Left*) and distal (light colors; *Right*) dendritic segments in glutamate-uncaging conditions (+ Glu). $^{**}P \leq 0.01$; $^{***}P \leq 0.001$; $^{****}P \leq 0.0001$; no symbol, $P > 0.05$. Statistical details are provided in *SI Appendix*, Table S1.

number per cluster, nanodomain area, or number of localizations (Fig. 2*F* and *SI Appendix*, Fig. S2 *F* and *G* and Table S1). Thus, interactions with CaMKII shape the nano-organization of GluN2B-NMDARs at proximal segments.

In line with these observations, single nanoparticle tracking revealed that preventing the interaction with CaMKII essentially affects GluN2B-NMDAR surface dynamics at proximal locations. Indeed, GluN2B-RSQD had lower instantaneous surface diffusion coefficient and surface explored values along with an increase in residency time within synaptic areas at proximal segments when compared with WT GluN2B-NMDARs (Fig. 2 *G* and *H*). Of note, a significant decrease in GluN2B-RSQD instantaneous surface diffusion coefficients was also observed at distal locations, although it was not associated with any change in synaptic residency time or surface explored (Fig. 2 *G* and *H* and *SI Appendix*, Fig. S2*H*). Collectively, these data suggest that interactions between CaMKII and GluN2B-NMDARs play an important role in shaping the nanoscale organization, surface mobility, and synaptic trapping of receptors at proximal segments.

Does this interplay require CaMKII activity? To address this question, we evaluated the impact of a specific inhibitor of CaMKII, Autocamtide-2-related inhibitory peptide (TAT-AIP), on the nanoscale organization of GluN2B-NMDARs at proximal segments (Fig. 2 *I* and *J* and *SI Appendix*, Fig. S3*A*). TAT-AIP–elicited inhibition of CaMKII resulted in a threefold increase in cluster local densities and a twofold increase in nanodomain local densities, respectively, compared with exposure to a control peptide, TAT-NS (Fig. 2*J* and *SI Appendix*, Fig. S3*B* and Table S1). To note, CaMKII inactivation also impacted the local densities of clusters and nanodomains of GluN2A-NMDARs, although to a lesser extent and without affecting cluster and nanodomain areas or numbers (*SI Appendix*, Fig. S3 *B–E* and Table S1), consistent with previously reported phosphorylation-based regulations (35, 64). Taken together, these results indicate that the nanoscale organization of GluN2B-NMDARs at proximal segments depends on a functional interplay and physical interaction with CaMKII.

Impact of the GluN2B-NMDAR/CaMKII Interplay on Long-Term Synaptic Potentiation along the Dendritic Tree. To explore the influence of GluN2B-NMDAR nanoscale organization on long-term plasticity rules along the dendritic tree, we expressed a SEP-tagged GluA1 AMPA receptor subunit and used a glutamate uncaging paradigm to induce LTP (61–63) at randomly selected proximal and distally located spines (Fig. 3*A*), measuring variations in SEP-GluA1 fluorescence intensity before and 20 min after uncaging as a readout of changes in AMPAR numbers and synaptic strength (Fig. 3 *B* and *C* and *SI Appendix*, Fig. S4*A*). Compared with the control condition (absence of caged-glutamate), glutamate uncaging resulted in the potentiation of 28% of the spines on average, with a mean 2.7-fold increase in potentiated spines that was prevented by the addition of AP5 and NBQX (Fig. 3*B* and *SI Appendix*, Table S1). LTP induction efficacy was comparable at proximal and distal spines (Fig. 3*C* and *SI Appendix*, Fig. S4*B* and Table S1), although 32% and 19% of spines on average were potentiated at proximal and

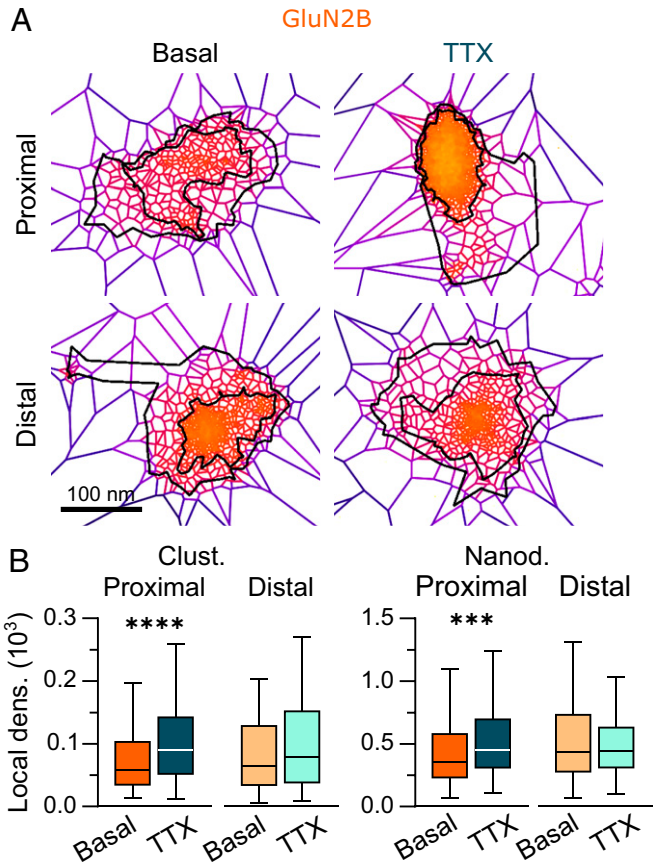

Fig. 4. GluN2B-NMDAR nanoscale organization is specifically altered at proximal dendritic segments by neuronal activity. (*A*) Representative GluN2B-NMDAR clusters in buffer (basal; *Left*) or after incubation with tetrodotoxin (TTX, 1 μM for 1 h; *Right*). (*B*) Local densities of GluN2B-NMDAR clusters and nanodomains at proximal (dark colors) and distal (light colors) dendritic segments in basal (orange) or TTX (cyan) conditions. Data are presented as box-and-whisker plots: line at median, IQR in box, whiskers represent minimum and maximum values. ***$P \leq 0.001$; ****$P \leq 0.0001$; no symbol, $P > 0.05$. Statistical details are provided in *SI Appendix*, Table S1.

distal spines, respectively. We then evaluated the impact of the interaction between GluN2B-NMDARs and CaMKII on LTP induction at proximal or distal sites by expressing either WT GluN2B-NMDARs or recombinant GluN2B-RSQD (Fig. 3*D* and *SI Appendix*, Fig. S4*B*). As was expected (29–36), preventing the interaction between the two partners significantly impaired LTP induction without completely occluding it (*SI Appendix*, Fig. S4*D* and Table S1). Interestingly, GluN2B-RSQD expression impaired LTP strongly at proximal spines and only moderately at distal spines (Fig. 3*E* and *SI Appendix*, Table S1), suggesting that the interaction between GluN2B-NMDARs and CaMKII plays a major role in the potentiation of proximal spines.

Neuronal Activity Regulates GluN2B-NMDAR Nanoscale Organization at Proximal Segments. Our results indicate that GluN2B-NMDARs at proximal segments are more prone to change their nanoscale organization through interaction with intracellular partners (54). To further explore this aspect, we tested whether a sustained decrease in neuronal activity (TTX; 1 h) comparably impacted GluN2B-NMDARs at proximal and distal segments (Fig. 4*A* and *SI Appendix*, Fig. S5*A*). We observed that inhibiting neuronal activity increased the number of nanodomains at both locations (*SI Appendix*, Fig. S5*C*); however, blocking neuronal activity triggered changes in the density of GluN2B-NMDAR clusters and nanodomains at proximal segments selectively through an increase in the number of localizations within GluN2B-NMDAR clusters and a decrease in the area of nanodomains at proximal segments (Fig. 4*B* and *SI Appendix*, Fig. S5*B* and Table S1). Of note, these changes are reminiscent of the rearrangements observed following CaMKII inhibition (Fig. 2 *I* and *J* and *SI Appendix*, Fig. S3) or disruption of the GluN2B/CaMKII interaction (Fig. 2 *E* and *F* and *SI Appendix*, Fig. S2 *E* and *F*). Thus, these results indicate that neuronal activity is required to maintain a relatively low density of GluN2B-NMDARs at proximal synapses.

Discussion

Hippocampal neurons receive and integrate a multitude of signals originating from synapses distributed along their dendritic arbor. Inputs located near the soma or at distal dendritic segments have different contributions to neuronal integration through a variety of mechanisms, including distinct NMDAR-dependent long-term plasticity processes. Here we used a combination of superresolution microscopy, single nanoparticle imaging, and glutamate uncaging to investigate the nanoscale organization and dynamics of GluN2A- and GluN2B-NMDARs along the dendritic tree of hippocampal pyramidal neurons and potential regulatory mechanisms and impact to the neuronal plasticity. We unveil that the nanoscale organization and surface dynamics of GluN2B-NMDARs, but not of GluN2A-NMDARs, changes between proximal and distal clusters with a gradual increase in receptor local density from proximal to distal dendritic segments. At proximal dendritic segments, the nanoscale organization and membrane dynamics of GluN2B-NMDARs are shaped by a physical interplay with CaMKII. Functionally, the nanoscale organization of GluN2B-NMDARs at proximal segments is tuned by neuronal activity and its interplay with CaMKII shapes activity-dependent synaptic potentiation. Thus, our results shed new light on how GluN2B-NMDAR distribution is regulated along the dendritic tree of hippocampal neurons and further highlights the intimate relationship between NMDAR dynamic organization and activity-dependent synaptic adaptations.

Glutamatergic synapses are distributed along the dendritic tree of hippocampal pyramidal cells, and mounting evidence indicate that synapses located at different dendritic segments display distinct morphological and functional properties (6, 65, 66). For instance, AMPAR-mediated synaptic transmission is higher at distal synapses when compared with proximal ones, a process that likely overcomes the dendritic filtering of excitatory postsynaptic potentials. Consistently, different contributions and/or compositions of NMDARs have been reported between proximal and distal synapses (37, 38, 40). As previously described in brain slices (11, 58, 59, 67), we confirmed that the area of the postsynaptic density (PSD) decreased as a function of distance from the soma. In addition, we unveiled that GluN2B-NMDARs display different nanoscale organization and surface mobility properties at proximal and distal synapses. At proximal dendritic segments, the organization and dynamics involve a functional and physical interplay between GluN2B-NMDARs and CaMKII and is regulated by neuronal activity. Intriguingly, physical interaction with CaMKII does not influence the nano-organization of GluN2B-NMDARs at distal segments, although both proteins are present in close proximity. Whether this results from the lower expression levels of CaMKII at distal locations or other mechanisms remains an open question. Of note, it has been suggested that mechanisms of CaMKII translocation and accumulation toward distal dendritic segments, through the stimulation of a small number of synapses, can indeed be independent of the binding to GluN2B-NMDARs (31, 63).

The key role of the GluN2B-NMDAR/CaMKII interaction at proximal segments suggests that these two proteins may

colocalize within functional nanodomains. However, when comparing the nanoscale organization of GluN2B-NMDARs and CaMKII, it appears that their basal distributions are different, irrespective of dendritic location. GluN2B-NMDARs were found to be clustered within delimited nanodomains, as described previously (49, 54). In contrast, CaMKII exhibited a widespread distribution. One may suggest that only a fraction of CaMKII coclusters with GluN2B-NMDARs. Further investigations are surely needed to shed additional light on the precise contribution of CaMKII to the synaptic organization of GluN2B-NMDARs and to further characterize the co-organization of both partners.

What could be the functional impact of such variations in the nanoscale organization of NMDARs? This question is central, as basal GluN2B-NMDAR–mediated current and calcium transient properties appear to be relatively stable along the dendritic arbor of pyramidal cells (40, 41). Could changes in receptor distribution and local density within nanodomains affect NMDAR-mediated transmission? Simulation studies seem to indicate that NMDAR activation is not extensively impacted by their organization into nanodomains (68), yet NMDAR currents are negatively coupled through calcium-dependent inactivation, and the degree of coupling is tuned by the distance between receptors; that is, NMDARs in close proximity efficiently inhibit one another (69). Thus, NMDARs at distal synapses are theoretically more prone to calcium-dependent inactivation, particularly when trains of action potentials trigger large local increases in intracellular calcium, and this strong compaction of distal receptors may have important consequences on NMDAR signaling.

Consistently, NMDAR-dependent synaptic plasticity rules vary between proximal and distal synapses (1, 5, 37, 38, 40, 46). While NMDAR-dependent LTP can successfully occur at both proximal and distal synapses, it is more easily induced at proximal synapses than at distal synapses in brain slices (42–45, 47). In contrast, distal synapses are more prone than proximal synapses to express stable forms of NMDAR-dependent LTD. Although the molecular mechanisms underpinning this disparity of long-term plasticity properties remain elusive, the observation that proximal and distal synapses feature different NMDAR nanoscale organizations and that the GluN2B/CaMKII interplay differently impacts plasticity expression at different dendritic locations may help us understand the origins of variations in NMDAR-dependent adaptation mechanisms.

Of interest, we recently demonstrated that manipulating the nanoscale organization of GluN2B-NMDARs without altering overall NMDAR-mediated currents drastically alters LTP expression (54). Besides the nanoscale density of NMDARs, it has been further demonstrated that LTP expression also requires a NMDAR- and mGluR5-dependent lateral escape of synaptic GluN2B-NMDARs (62, 70). Blocking this surface relocation or genetically preventing the interaction between GluN2B and CaMKII prevents the activity-dependent accumulation of CaMKII at spines and occluded LTP, raising the possibility that GluN2B-NMDAR act as a cargo for CaMKII during synaptic plasticity initiation (29, 32, 62, 71). Since the interaction between GluN2B-NMDARs and CaMKII is central for the nanoscale organization of NMDARs at proximal dendritic segments as well as for the induction of LTP, we propose that the functional interplay between GluN2B-NMDARs and CaMKII tunes LTP through the mutual regulation of both their biophysical properties and their local trafficking. Together with past studies, these new data fuel a model in which the nanoscale organization and membrane dynamics of GluN2B-NMDARs are differently set along the dendritic tree. At proximal segments, neuronal activity would keep a large pool of GluN2B-NMDARs at low density and in a highly dynamic state, favoring subsequent long-term synaptic plasticity processes. Thus, depending on the localization along the dendritic arbor, the nanoscale organization of NMDARs and associated signaling partners such as CaMKII likely shapes the plastic behaviors of proximal and distal inputs and tunes their leverage on neuronal integration.

Materials and Methods

Detailed descriptions of the experimental procedures and analyses are provided in *SI Appendix, Materials and Methods*. In brief, hippocampal neurons were immunostained and imaged by dSTORM for quantitative analysis of the nanoscale organization of receptors and CaMKII. Single-particle tracking was performed using quantum-dots coupled to anti-rabbit secondary antibodies. LTP was evoked using local one-photon uncaging of glutamate (20 pulses, 0.5 Hz). The use of animals for hippocampal culture preparation was in accordance with protocols approved by Ethical Committee No. 50 of the University of Bordeaux, attached to the National Center for Ethical Reflection on Animal Experiments.

Data Availability. All study data are included in the main text and *SI Appendix*.

ACKNOWLEDGMENTS. We thank Magali Mondin and Sébastien Marais and all the staff of the Bordeaux Imaging Center, a service unit of the CNRS-INSERM and University of Bordeaux and a member of the national infrastructure France BioImaging (ANR-10-INBS-04-01). We also thank Emeline Verdier and Elise Goyet for help with cell cultures and molecular biology; Ana Luísa Carvalho (Center of Neuroscience and Cell Biology; University of Coimbra) and Ann Marie Craig (Djavad Mowafaghian Centre for Brain Health, University of British Columbia) for the YFP-GluN2A and -2B original plasmids; and Paul De Koninck (University of Laval) for the alpha CaMKII plasmid. This work was supported by the CNRS, Agence Nationale de la Recherche (ANR-14-OHRI-0001-01, ANR-15-CE16-0004-03, and ANR-16-CE13-0018), IdEx Bordeaux (ANR-10-IDEX-03-02), Fondation pour la Recherche Médicale, Human Frontiers Science Program (RGP0019), Conseil Régional d'Aquitaine, and Labex Bordeaux BRAIN.

1. R. Kajiwara *et al*., Convergence of entorhinal and CA3 inputs onto pyramidal neurons and interneurons in hippocampal area CA1: An anatomical study in the rat. *Hippocampus* **18**, 266–280 (2008).
2. N. Spruston, Pyramidal neurons: Dendritic structure and synaptic integration. *Nat. Rev. Neurosci.* **9**, 206–221 (2008).
3. J. Basu, S. A. Siegelbaum, The corticohippocampal circuit, synaptic plasticity, and memory. *Cold Spring Harb. Perspect. Biol.* **7**, a021733 (2015).
4. N. M. van Strien, N. L. M. Cappaert, M. P. Witter, The anatomy of memory: An interactive overview of the parahippocampal-hippocampal network. *Nat. Rev. Neurosci.* **10**, 272–282 (2009).
5. V. A. Alvarez, B. L. Sabatini, Anatomical and physiological plasticity of dendritic spines. *Annu. Rev. Neurosci.* **30**, 79–97 (2007).
6. T. Branco, M. Häusser, The single dendritic branch as a fundamental functional unit in the nervous system. *Curr. Opin. Neurobiol.* **20**, 494–502 (2010).
7. J. C. Magee, E. P. Cook, Somatic EPSP amplitude is independent of synapse location in hippocampal pyramidal neurons. *Nat. Neurosci.* **3**, 895–903 (2000).
8. B. K. Andrásfalvy, J. C. Magee, Distance-dependent increase in AMPA receptor number in the dendrites of adult hippocampal CA1 pyramidal neurons. *J. Neurosci.* **21**, 9151–9159 (2001).
9. M. A. Smith, G. C. R. Ellis-Davies, J. C. Magee, Mechanism of the distance-dependent scaling of Schaffer collateral synapses in rat CA1 pyramidal neurons. *J. Physiol.* **548**, 245–258 (2003).
10. M. F. Nolan *et al*., A behavioral role for dendritic integration: HCN1 channels constrain spatial memory and plasticity at inputs to distal dendrites of CA1 pyramidal neurons. *Cell* **119**, 719–732 (2004).
11. D. A. Nicholson *et al*., Distance-dependent differences in synapse number and AMPA receptor expression in hippocampal CA1 pyramidal neurons. *Neuron* **50**, 431–442 (2006).
12. A. Losonczy, J. K. Makara, J. C. Magee, Compartmentalized dendritic plasticity and input feature storage in neurons. *Nature* **452**, 436–441 (2008).
13. D. A. Nicholson, Y. Geinisman, Axospinous synaptic subtype-specific differences in structure, size, ionotropic receptor expression, and connectivity in apical dendritic regions of rat hippocampal CA1 pyramidal neurons. *J. Comp. Neurol.* **512**, 399–418 (2009).
14. M. S. Ahmed, S. A. Siegelbaum, Recruitment of N-type Ca(2+) channels during LTP enhances low release efficacy of hippocampal CA1 perforant path synapses. *Neuron* **63**, 372–385 (2009).
15. S. L. Shipman, B. E. Herring, Y. H. Suh, K. W. Roche, R. A. Nicoll, Distance-dependent scaling of AMPARs is cell-autonomous and GluA2- dependent. *J. Neurosci.* **33**, 13312–13319 (2013).
16. V. Menon *et al*., Balanced synaptic impact via distance-dependent synapse distribution and complementary expression of AMPARs and NMDARs in hippocampal dendrites. *Neuron* **80**, 1451–1463 (2013).

17. P. Paoletti, C. Bellone, Q. Zhou, NMDA receptor subunit diversity: Impact on receptor properties, synaptic plasticity and disease. *Nat. Rev. Neurosci.* **14**, 383–400 (2013).
18. K. Yashiro, B. D. Philpot, Regulation of NMDA receptor subunit expression and its implications for LTD, LTP, and metaplasticity. *Neuropharmacology* **55**, 1081–1094 (2008).
19. I. Ito, R. Kawakami, K. Sakimura, M. Mishina, H. Sugiyama, Input-specific targeting of NMDA receptor subtypes at mouse hippocampal CA3 pyramidal neuron synapses. *Neuropharmacology* **39**, 943–951 (2000).
20. C.-C. C. Wang *et al*., A critical role for GluN2B-containing NMDA receptors in cortical development and function. *Neuron* **72**, 789–805 (2011).
21. S. B. Mierau, R. M. Meredith, A. L. Upton, O. Paulsen, Dissociation of experience-dependent and -independent changes in excitatory synaptic transmission during development of barrel cortex. *Proc. Natl. Acad. Sci. U.S.A.* **101**, 15518–15523 (2004).
22. R. Kawakami, Asymmetrical allocation of NMDA receptor epsilon2 subunits in hippocampal circuitry. *Science* **300**, 990–994 (2003).
23. C. G. Lau, R. S. Zukin, NMDA receptor trafficking in synaptic plasticity and neuropsychiatric disorders. *Nat. Rev. Neurosci.* **8**, 413–426 (2007).
24. C. C. Smith, L. C. Vedder, L. L. McMahon, Estradiol and the relationship between dendritic spines, NR2B-containing NMDA receptors, and the magnitude of long-term potentiation at hippocampal CA3-CA1 synapses. *Psychoneuroendocrinology* **34** (suppl 1), S130–S142 (2009).
25. K. Akashi *et al*., NMDA receptor GluN2B (GluR epsilon 2/NR2B) subunit is crucial for channel function, postsynaptic macromolecular organization, and actin cytoskeleton at hippocampal CA3 synapses. *J. Neurosci.* **29**, 10869–10882 (2009).
26. J. S. Espinosa, D. G. Wheeler, R. W. Tsien, L. Luo, Uncoupling dendrite growth and patterning: Single-cell knockout analysis of NMDA receptor 2B. *Neuron* **62**, 205–217 (2009).
27. J. A. Gray *et al*., Distinct modes of AMPA receptor suppression at developing synapses by GluN2A and GluN2B: Single-cell NMDA receptor subunit deletion in vivo. *Neuron* **71**, 1085–1101 (2011).
28. J. A. Matta, M. C. Ashby, A. Sanz-Clemente, K. W. Roche, J. T. R. Isaac, mGluR5 and NMDA receptors drive the experience- and activity-dependent NMDA receptor NR2B to NR2A subunit switch. *Neuron* **70**, 339–351 (2011).
29. J. Lisman, R. Yasuda, S. Raghavachari, Mechanisms of CaMKII action in long-term potentiation. *Nat. Rev. Neurosci.* **13**, 169–182 (2012).
30. K. Shen, Dynamic control of CaMKII translocation and localization in hippocampal neurons by NMDA receptor stimulation. *Science* **284**, 162–167 (1999).
31. K. She, J. K. Rose, A. M. Craig, Differential stimulus-dependent synaptic recruitment of CaMKIIα by intracellular determinants of GluN2B. *Mol. Cell. Neurosci.* **51**, 68–78 (2012).
32. N. Otmakhov *et al*., Persistent accumulation of calcium/calmodulin-dependent protein kinase II in dendritic spines after induction of NMDA receptor-dependent chemical long-term potentiation. *J. Neurosci.* **24**, 9324–9331 (2004).
33. A. R. Halt *et al*., CaMKII binding to GluN2B is critical during memory consolidation. *EMBO J.* **31**, 1203–1216 (2012).
34. A. Barria, R. Malinow, NMDA receptor subunit composition controls synaptic plasticity by regulating binding to CaMKII. *Neuron* **48**, 289–301 (2005).
35. K. U. Bayer, H. Schulman, CaM kinase: Still inspiring at 40. *Neuron* **103**, 380–394 (2019).
36. M. Sanhueza, J. Lisman, The CaMKII/NMDAR complex as a molecular memory. *Mol. Brain* **6**, 10 (2013).
37. A. S. Walker *et al*., Distance-dependent gradient in NMDAR-driven spine calcium signals along tapering dendrites. *Proc. Natl. Acad. Sci. U.S.A.* **114**, E1986–E1995 (2017).
38. N. A. Otmakhova, N. Otmakhov, J. E. Lisman, Pathway-specific properties of AMPA- and NMDA-mediated transmission in CA1 hippocampal pyramidal cells. *J. Neurosci.* **22**, 1199–1207 (2002).
39. E. Arrigoni, R. W. Greene, Schaffer collateral and perforant path inputs activate different subtypes of NMDA receptors on the same CA1 pyramidal cell. *Br. J. Pharmacol.* **142**, 317–322 (2004).
40. J. A. Varela, S. J. Hirsch, D. Chapman, L. S. Leverich, R. W. Greene, D1/D5 modulation of synaptic NMDA receptor currents. *J. Neurosci.* **29**, 3109–3119 (2009).
41. S. R. Metzbower, Y. Joo, D. R. Benavides, T. A. Blanpied, Properties of individual hippocampal synapses influencing NMDA-receptor activation by spontaneous neurotransmission. *Eneuro* **6**, ENEURO.0419-18.2019 (2019).
42. O. Paulsen, Y.-G. Li, O. Hvalby, P. Anderson, T. V. P. Bliss, Failure to induce long-term depression by an anti-correlation procedure in area CA1 of the rat hippocampal slice. *Eur. J. Neurosci.* **5**, 1241–1246 (1993).
43. S. Parvez, B. Ramachandran, J. U. Frey, Functional differences between and across different regions of the apical branch of hippocampal CA1 dendrites with respect to long-term depression induction and synaptic cross-tagging. *J. Neurosci.* **30**, 5118–5123 (2010).
44. S. Sajikumar, M. Korte, Metaplasticity governs compartmentalization of synaptic tagging and capture through brain-derived neurotrophic factor (BDNF) and protein kinase Mzeta (PKMzeta). *Proc. Natl. Acad. Sci. U.S.A.* **108**, 2551–2556 (2011).
45. E. B. Han, S. F. Heinemann, Distal dendritic inputs control neuronal activity by heterosynaptic potentiation of proximal inputs. *J. Neurosci.* **33**, 1314–1325 (2013).
46. A. Aksoy-Aksel, D. Manahan-Vaughan, The temporoammonic input to the hippocampal CA1 region displays distinctly different synaptic plasticity compared to the Schaffer collateral input in vivo: Significance for synaptic information processing. *Front. Synaptic Neurosci.* **5**, 5 (2013).
47. B. Ramachandran, S. Ahmed, N. Zafar, C. Dean, Ethanol inhibits long-term potentiation in hippocampal CA1 neurons, irrespective of lamina and stimulus strength, through neurosteroidogenesis. *Hippocampus* **25**, 106–118 (2015).
48. B. Huang, M. Bates, X. Zhuang, Super-resolution fluorescence microscopy. *Annu. Rev. Biochem.* **78**, 993–1016 (2009).
49. H. D. MacGillavry, Y. Song, S. Raghavachari, T. A. Blanpied, Nanoscale scaffolding domains within the postsynaptic density concentrate synaptic AMPA receptors. *Neuron* **78**, 615–622 (2013).
50. D. Nair *et al*., Super-resolution imaging reveals that AMPA receptors inside synapses are dynamically organized in nanodomains regulated by PSD95. *J. Neurosci.* **33**, 13204–13224 (2013).
51. C. G. Specht *et al*., Quantitative nanoscopy of inhibitory synapses: Counting gephyrin molecules and receptor binding sites. *Neuron* **79**, 308–321 (2013).
52. F. Pennacchietti *et al*., Nanoscale molecular reorganization of the inhibitory postsynaptic density is a determinant of GABAergic synaptic potentiation. *J. Neurosci.* **37**, 1747–1756 (2017).
53. A.-H. Tang *et al*., A trans-synaptic nanocolumn aligns neurotransmitter release to receptors. *Nature* **536**, 210–214 (2016).
54. B. Kellermayer *et al*., Differential nanoscale topography and functional role of GluN2-NMDA receptor subtypes at glutamatergic synapses. *Neuron* **100**, 106–119.e7 (2018).
55. K. T. Haas *et al*., Pre-post synaptic alignment through neuroligin-1 tunes synaptic transmission efficiency. *eLife* **7**, 1–22 (2018).
56. M. Hruska, N. Henderson, S. J. Le Marchand, H. Jafri, M. B. Dalva, Synaptic nanomodules underlie the organization and plasticity of spine synapses. *Nat. Neurosci.* **21**, 671–682 (2018).
57. M. Hruska, N. T. Henderson, N. L. Xia, S. J. Le Marchand, M. B. Dalva, Anchoring and synaptic stability of PSD-95 is driven by ephrin-B3. *Nat. Neurosci.* **18**, 1594–1605 (2015).
58. Y. Katz *et al*., Synapse distribution suggests a two-stage model of dendritic integration in CA1 pyramidal neurons. *Neuron* **63**, 171–177 (2009).
59. F. W. Grillo *et al*., A distance-dependent distribution of presynaptic boutons tunes frequency-dependent dendritic integration. *Neuron* **99**, 275–282.e3 (2018).
60. F. Levet *et al*., SR-Tesseler: A method to segment and quantify localization-based super-resolution microscopy data. *Nat. Methods* **12**, 1065–1071 (2015).
61. M. J. Broadhead *et al*., PSD95 nanoclusters are postsynaptic building blocks in hippocampus circuits. *Sci. Rep.* **6**, 24626 (2016).
62. J. P. Dupuis *et al*., Surface dynamics of GluN2B-NMDA receptors controls plasticity of maturing glutamate synapses. *EMBO J.* **33**, 842–861 (2014).
63. J. Rose, S.-X. Jin, A. M. Craig, Heterosynaptic molecular dynamics: Locally induced propagating synaptic accumulation of CaM kinase II. *Neuron* **61**, 351–358 (2009).
64. M. P. Lussier, A. Sanz-Clemente, K. W. Roche, Dynamic regulation of N-methyl-D-aspartate (NMDA) and α-amino-3-hydroxy-5-methyl-4-isoxazolepropionic acid (AMPA) receptors by posttranslational modifications. *J. Biol. Chem.* **290**, 28596–28603 (2015).
65. T. Branco, M. Häusser, Synaptic integration gradients in single cortical pyramidal cell dendrites. *Neuron* **69**, 885–892 (2011).
66. T. Klausberger, P. Somogyi, Neuronal diversity and temporal dynamics: The unity of hippocampal circuit operations. *Science* **321**, 53–57 (2008).
67. W. Wegner, A. C. Mott, S. G. N. Grant, H. Steffens, K. I. Willig, In vivo STED microscopy visualizes PSD95 sub-structures and morphological changes over several hours in the mouse visual cortex. *Sci. Rep.* **8**, 219 (2018).
68. J. Goncalves *et al*., Nanoscale co-organization and coactivation of AMPAR, NMDAR, and mGluR at excitatory synapses. *Proc. Natl. Acad. Sci. U.S.A.* **117**, 14503–14511 (2020).
69. G. J. Iacobucci, G. K. Popescu, Spatial coupling tunes NMDA receptor responses via Ca^{2+} diffusion. *J. Neurosci.* **39**, 8831–8844 (2019).
70. C. Bellone, M. Mameli, C. Lüscher, In utero exposure to cocaine delays postnatal synaptic maturation of glutamatergic transmission in the VTA. *Nat. Neurosci.* **14**, 1439–1446 (2011).
71. K.-U. Bayer, P. De Koninck, A. S. Leonard, J. W. Hell, H. Schulman, Interaction with the NMDA receptor locks CaMKII in an active conformation. *Nature* **411**, 801–805 (2001).